**Supporting Information for *Structure of an Oxalate Oxidoreductase Provides Insight into Microbial 2-Oxoacid Metabolism***

**Table S1**. Data Collection and Model Refinement Statistics

| | MAD OOR | | | OOR |
|---|---|---|---|---|
| Data collection and processing | | | | |
| Space group | $P2_12_12_1$ | $P2_12_12_1$ | $P2_12_12_1$ | $P2_12_12_1$ |
| Cell dimensions (Å) | 114, 145, 163 | 114, 145, 163 | 114, 145, 163 | 84, 152, 172 |
| Dataset | Peak[a] | Inflection | Remote | |
| Wavelength (Å) | 1.73600 | 1.74210 | 1.64390 | 0.97950 |
| Resolution (Å) | 50.0 – 3.50 (3.56 – 3.50)[b] | 50.0 – 3.80 (3.87 – 3.80) | 50.0 – 3.75 (3.81 – 3.75) | 48.7 – 2.27 (2.35 – 2.27) |
| Total unique reflections | 50,206 | 22,059 | 24,672 | 82,301 |
| Completeness (%) | 77.6 (44.9) | 81.9 (62.4) | 87.1 (82.5) | 81.1 (50.8) |
| Redundancy | 4.4 (4.1) | 4.8 (4.6) | 5.0 (5.0) | 5.6 (4.4) |
| $\langle I/\sigma I \rangle$ | 10.7 (2.3) | 12.2 (2.3) | 14.4 (2.1) | 6.5 (2.7) |
| $R_{sym}$[c] (%) | 10.9 (54.1) | 10.9 (48.8) | 10.1 (54.1) | 17.1 (57.7) |
| $CC_{1/2}$ (%) | [d] | [d] | [d] | 78.8 |
| Model Refinement | | | | |
| R-work (%) | | | | 17.4 |
| R-free (%) | | | | 21.6 |
| Protein atoms | | | | 15546 |
| TPP-$Mg^{2+}$ atoms | | | | 54 |
| [4Fe-4S] atoms | | | | 48 |
| Water molecules | | | | 1636 |
| RMS(bonds) (Å) | | | | 0.007 |
| RMS(angles) (°) | | | | 1.44 |
| Ramachandran favored (%) | | | | 97.0 |
| Ramachandran allowed (%) | | | | 2.8 |
| Ramachandran outliers (%) | | | | 0.2 |
| Average *B*-factor ($Å^2$) | | | | 22.40 |
| Protein ($Å^2$) | | | | 22.20 |
| TPP-$Mg^{2+}$ ($Å^2$) | | | | 21.82 |
| [4Fe-4S] ($Å^2$) | | | | 10.58 |
| Water ($Å^2$) | | | | 26.40 |

[a]The peak dataset was scaled anomalously to keep non-equivalent Bijvoet pairs separate. Bijvoet pairs for the inflection and remote datasets were merged.
[b]Numbers in parentheses indicate the highest resolution bin.
[c]$\Sigma(|I - \langle I \rangle|)/\Sigma(I)$
[d]The version of HKL2000 used to scale these datasets did not report $CC_{1/2}$

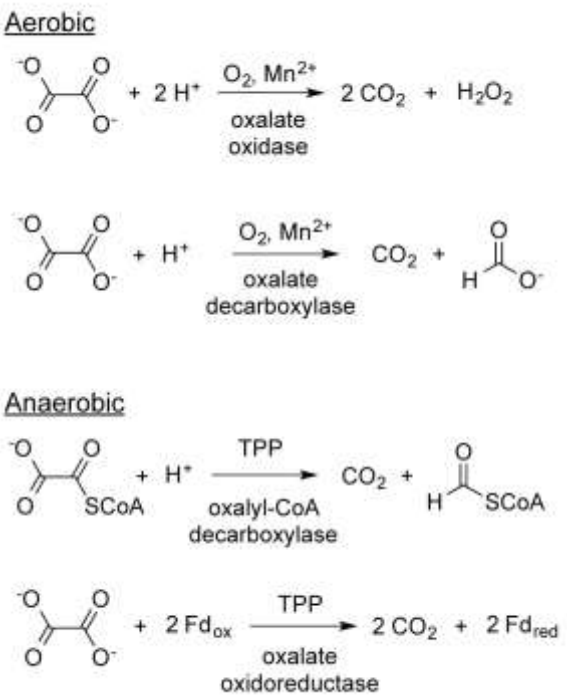


**Figure S1**. There are four known enzymatic reactions that consume oxalate in nature. Above, the two aerobic reactions are catalyzed by $Mn^{2+}$ and $O_2$. Below, the two anaerobic reactions are catalyzed by TPP.

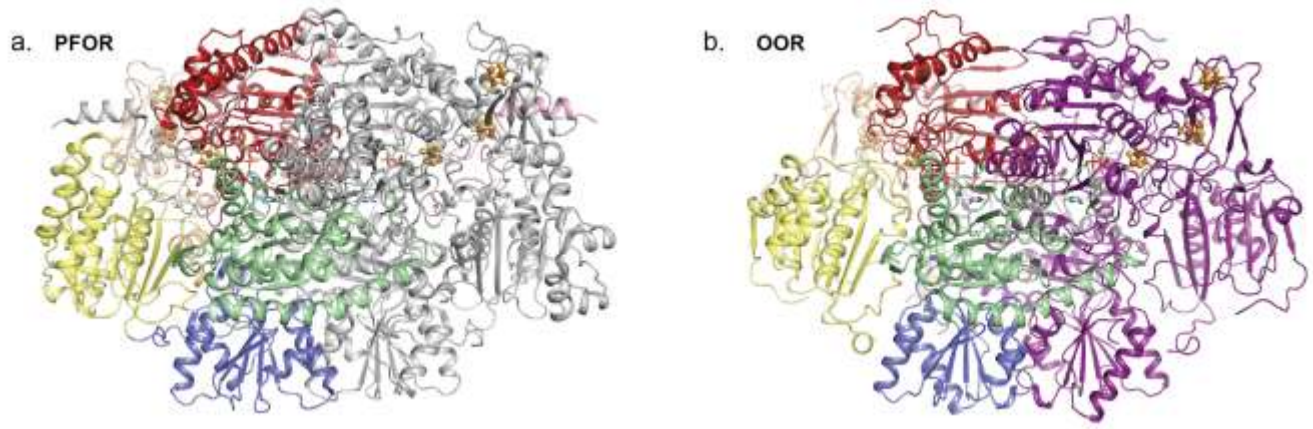


**Figure S2**. Side-by-side comparison of *D. africanus* PFOR and *M. thermoacetica* OOR. **a)** The PFOR $\alpha_2$ dimer (PDB-ID: 2C42) is shown in ribbon representation, with the right monomer colored gray, and the left monomer colored by domain as follows: I – green, II – blue, III – yellow, IV – orange, V – wheat, VI – red, and VII, pink. **b)** The OOR $(\alpha\gamma\beta)_2$ dimer is shown as in Figure 2a.

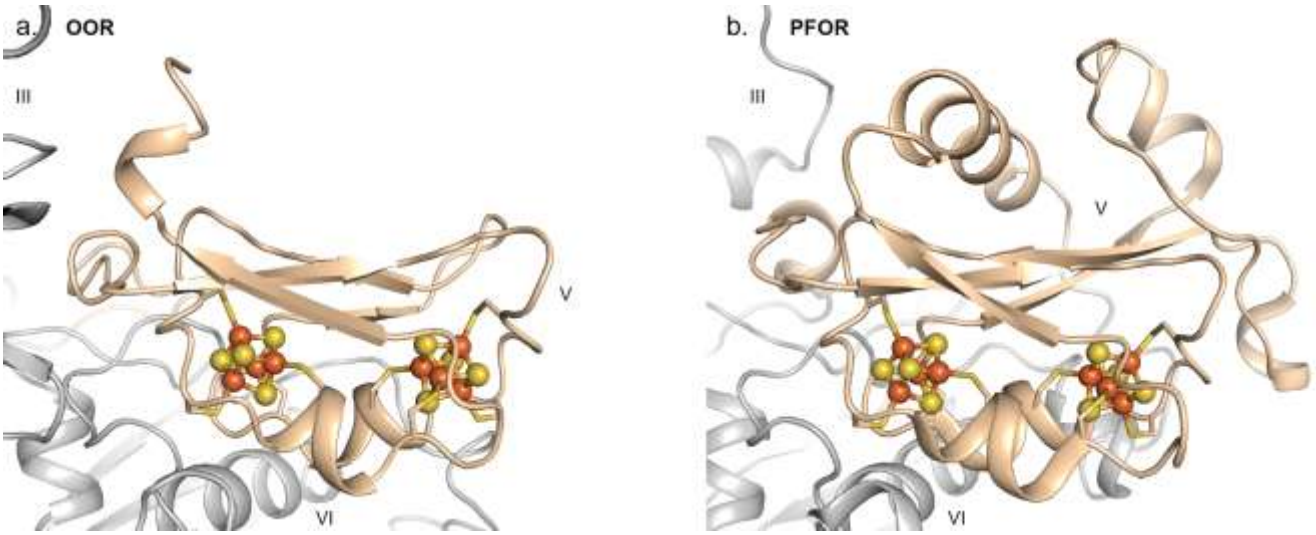


**Figure S3**. Comparison of ferredoxin domains between OOR and *Da* PFOR (PDB-ID: 2C42). **a)** Domain V from OOR is shown in ribbon representation and colored wheat. It is flanked by domains III on the left and IV on the bottom, colored gray. The medial (left) and distal (right) [4Fe-4S] clusters are shown in ball-and-stick representation. **b)** Domain V from PFOR is shown in ribbon representation and colored wheat. It is flanked by domains III on the left and IV on the bottom, colored gray. The medial (left) and distal (right) [4Fe-4S] clusters are shown in ball-and-stick representation. Two insertions above and right of the core ferredoxin fold create a substantially different protein surface to that in OOR.

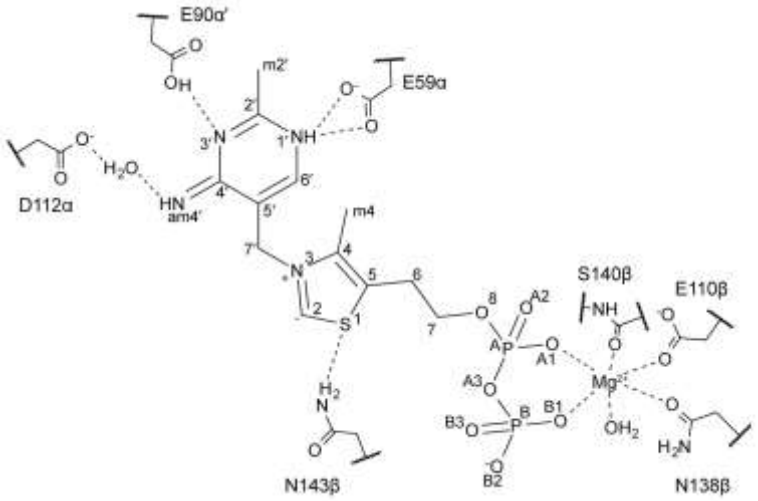


**Potential hydrogen bonding to TPP**

| TPP atom | H-bond partner residue | H-bond type | Distance |
|---|---|---|---|
| S1 | N143β | N-H-S | 4.2 Å |
| N1′ | E59α | N-H-O | 2.9 Å |
| N3′ | E90α′ | N-H-O | 4.0 Å |
| Nam4′ | $H_2O$ | N-H-O | 2.8 Å |

**Figure S4**. Numbering scheme in TPP and its immediate environment. Thiamine pyrophosphate is shown in the ylide form with C2 deprotonated, with atoms numbered for reference. The mode of binding of the pyrophosphates to $Mg^{2+}$, as well as the rest of the $Mg^{2+}$ coordination sphere, is shown. Potential hydrogen-bonding interactions between the thiazole and pyrimidine rings of TPP and the surrounding environment are indicated by dashed lines. Protonation states are hypothesized. Distances between residues in the OOR crystal structure are indicated in the table.

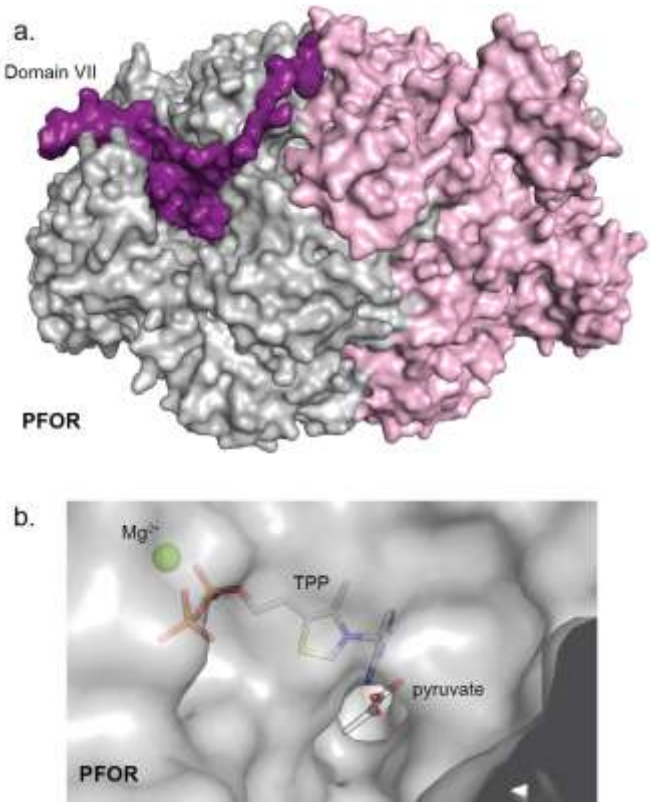


**Figure S5**. Domain VII of *Da* PFOR (PDB-ID: 2C42). **a)** The PFOR $\alpha_2$ dimer is shown in surface representation. The left monomer is colored gray. The right monomer is shown with domains I-VI in pink and domain VII in purple. Domain VII wraps around the left monomer and fills in a cavity that leads directly to the active site of the neighboring monomer. **b)** PFOR is shown as a gray semitransparent surface, with TPP and pyruvate shown as sticks, and $Mg^{2+}$ shown as a green sphere. When domain VII′ (from the opposite monomer) is omitted from the model, a direct solvent channel to the active site of PFOR opens up, which is a likely location for CoA binding.


**Figure S6.** Alignment of proximal-cluster-binding residues from domain VI of various OFORs. The conserved CXGC motif spans enzymes of this family (oxalate oxidoreductase (OOR), pyruvate:ferredoxin oxidoreductase (PFOR), isovalerate oxidoreductase (VOR), α-ketoglutarate oxidoreductase (KGOR), and indolepyruvate oxidoreductase (IOR)) across all branches of life. On the left, a tree indicates the relationship between each of the enzymes, calculated by maximum likelihood using a Blossom62 model of amino acid substitution,[1] from 125 residues in conserved blocks. Species (with Uniprot accession codes) included are: *Moorella thermoacetica (Q2RI42, Q2RMD6, Q2RH06), Thermotoga maritime (Q56317), Pyrococcus furiosus (Q51805, Q51802, I6V0T7), Thermococcus litoralis (H3ZKI0, H3ZPH4, H3ZL62), Thauera aromatica (Q8RJQ9), Giardia intestinalis (Q24982), Trichomonas vaginalis (Q27089), Enterobacter agglomerans (P19543),* and *Desulfovibrio africanus (P94692).*

## References

(1) Guindon, S.; Gascuel, O. A Simple, Fast, and Accurate Algorithm to Estimate Large Phylogenies by Maximum Likelihood. *Syst. Biol.* **2003**, *52* (5), 696–704.